Observation of melt ejection in metals up to 1 μs after femtosecond laser irradiation by a novel pump-probe photography setup

I. Mingareev, A. Horn and E.W. Kreutz
Lehrstuhl für Lasertechnik, RWTH Aachen, Steinbachstraße 15, 52074 Aachen, Germany

ABSTRACT

Irradiation of metals with ultrashort laser pulses reveals a variety of versatile microscopic processes compared to longer pulses. In particular, the impact of some material-specific characteristics, such as the electron-phonon coupling, seems to get more significance in order to meet the machining requirements. Finding the optimal process parameter area has been therefore a dominating problem in materials processing with sub-picosecond laser radiation.

Ablation of bulk metals (Al, Cu) has been investigated in-situ by means of high-resolution pump-probe photography using pump laser radiation of pulse duration t_p=80 fs, at wavelength of 820 nm. This technique enables direct visualization of laser-induced processes up to 1 μs after the interaction of a single laser pulse with material. Variation of the fluence of the laser radiation, behavior and time characteristics of melting and post-melting processes have been matter of research.

Depending on metal-specific parameters, qualitatively different ablation phenomena have been observed. Structural analysis by electron and optical microscopies reveals rosette-like surface structures showing the morphology of the ablated regions. The temporal development of the ablation dynamics can be conditionally categorized into different characteristic time regions. Particularly, laser induced melt injection has been observed in the time range of 700 ns to 1.0 μs after the initial laser-metal interaction.

Keywords: femtosecond ablation, laser processing, delay line, melt ejection, high-speed photography

1. INTRODUCTION

The interaction of femtosecond laser radiation with different materials is now intensively studied in many laboratories around the world. It is accepted that femtosecond laser radiation gives two major advantages to micromachining compared to nanosecond and longer pulses: (i) the reduction of the pulse energy which is necessary to induce ablation for fixed laser wavelength and focusing conditions, and (ii) a significant reduction of heat-affected zone (HAZ) and, as consequence, the improvement of the contour sharpness for the laser-processed structures. The second advantage is a direct consequence of the pulse duration being much smaller than the heat diffusion time. Improved availability and compactness of ultra-short, sub-ps pulsed solid-state lasers has stimulated a growing interest in the exploiting of the enhanced flexibility of femtosecond technology for micro-machining. Disregarding price and user friendliness of present laser systems – which will improve massively in the coming years – ultra-short laser pulses offer a variety of advantages for precision micro-fabrication. Numerous materials like metals[1,2], semiconductors[3], ceramics[4], dielectrics[5] and composite materials[6] have been investigated. However, many aspects of the femtosecond ablation remain unclear, while the regimes of the processing of some industrially important materials are not yet optimized.

The absence of a quantitative model at least in part contributes to the lack of understanding of femtosecond laser ablation. On the other hand, systematic time-resolved measurements can help to establish more predictive theories for laser ablation on the femtosecond time scale.

Alternative visualization techniques, e.g. photography by ICCD or high-speed CCD cameras, feature low applicability to image transient processes, providing low spatial and/or temporal resolution. Ultrafast time-resolved optical shadowgraphy combines pump-probe technique with optical microscopy, allowing time- and space-resolved measurements of the changes in the material morphology induced by the laser excitation pulse. The temporal resolution

High-Power Laser Ablation VI, edited by Claude R. Phipps, Proc. of SPIE
Vol. 6261, 62610A, (2006) · 0277-786X/06/$15 · doi: 10.1117/12.669350

Downloaded From: http://proceedings.spiedigitallibrary.org/ on 12/29/2015 Terms of Use: http://spiedigitallibrary.org/ss/TermsOfUse.aspx

is given by the duration of the probe pulse, typically around 100 fs. The spatial resolution is determined by the properties of the imaging optics, e.g. numerical aperture and magnification, and can be of the order of a micrometer. Generally, the temporal detection region is technically limited by the delay stage used in the experimental setup. A low-loss multi-pass delay stage presented in this paper enables time delays up to 1.2 µs preserving small pulse duration of the probe laser radiation. This delay stage provides the key feature of the experimental setup.

In this work, some of the characteristics resulting from femtosecond laser ablation of bulk metals will be elucidated by means of direct visualization techniques such as shadowgraphy. A detailed examination of the development of laser ablation dynamics on aluminium and copper surfaces on the femtosecond to microsecond time scale is presented. This paper is organized as follows. Section 2 presents the femtosecond time-resolved experimental system and the design of the multi-pass delay stage. Images of ablation processes made by this novel pump-probe technique are presented in section 3. The investigations comprise effects that occur when highly pressurized, heated material expands and transforms into gaseous and liquid states. Here, time resolved shadowgraphy presents a universal instrument for evaluation of the ablation processes for a variety of materials at energies close to the ablation threshold.

2. EXPERIMENTAL

2.1 Laser, optics and experimental methodology

Laser ablation experiments were performed using a femtosecond time-resolved pump-probe setup (Figure 1) to image the emission of particles, vapor and melt. A femtosecond CPA-laser system (Thales Concerto) operated in single pulse mode at the wavelength λ=820 nm was used as the pump (processing) laser radiation, which has a pulse duration of 80 fs (FWHM), nearly Gaussian beam profile and energy output up to 1.5 mJ per pulse. The laser radiation is focused by a microscope objective L1 (Olympus MSPlan20, NA = 0.4) to a calculated spot size of about 10 µm with a magnification of 20x. The applied pulse energy constitutes up to six times the ablation threshold for each material under investigation. After a beam splitter, the laser radiation passes a multi-pass optical delay stage and a 2ω or white light continuum (WLC) generator, forming a probe beam (L2, L3) that is perpendicular to the optical axis of the pump laser radiation. By adjusting the multi-pass delay stage on an optical rail and by use of an additional linear delay stage for the pump laser radiation, the optical paths of the pump and probe beams can be continuously varied. So the time difference between the initial pump pulse and the sample illumination is changed.

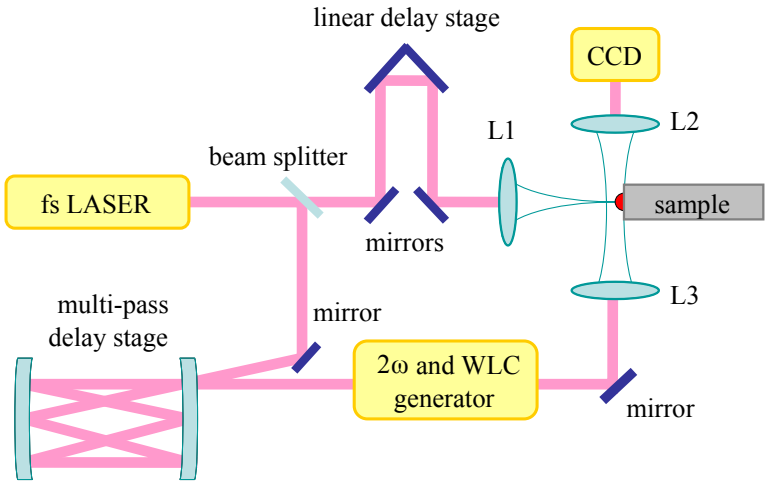

Figure 1. Schematic setup of the femtosecond pump-probe experiment.

About 10x10x1 mm sized, polished Al or Cu samples with optical quality featuring high chemical purity (>99.9%) can be flexibly moved by three high-precision stages (Physikinstrumente). Shadowgraphs are taken by a CCD camera (Baumer Optronic arc4000c), using a microscope objective L2 (Olympus MSPlan50, NA = 0.55) with the overall spatial resolution of 1.5 µm. Spatial transmittance images can be obtained by dividing the shadowgraph intensities during laser

Downloaded From: http://proceedings.spiedigitallibrary.org/ on 12/29/2015 Terms of Use: http://spiedigitallibrary.org/ss/TermsOfUse.aspx

irradiation of the sample with background intensities without laser excitation. This experimental setup enables setting time delays up to 1.2 μs with the time resolution of about 100 fs and can be used for observation of transient processes both on surfaces and inside transparent materials. Ex-situ measurements of the induced surface morphology are performed with scanning electron microscopy (SEM).

2.2 Design of the multi-pass delay stage

A multi-pass delay stage with two concave mirrors, also called Herriott cell, was designed to obtain extra long optical paths. The Herriott cell allows a number of beam geometries useful for various applications such as interferometry, long path spectroscopy, high precision optical loss measurements and multi-pass laser cavities. The key advantages of the use of multi-pass delay stage for femtosecond pump-probe experiments include: (i) keeping pulse duration constant and, therefore, short illumination times due to nearly zero-chirp concave mirrors, and (ii) preserving of the beam divergence, as a result of periodic focusing inside the cavity, using appropriate design conditions. In combination with a precise linear delay stage (Figure 1), any delay values within the time range between about 100 fs and 1.2 μs can be investigated.

In its simplest form, a Herriott cell based delay stage consists of a stable two-mirror resonator and a mechanism for injecting and extracting light beams, for example by use of additional flat or curved mirrors, holes or slits in one or both of the mirrors. When the Herriott cell parameters are properly adjusted, the incident beam injected with the correct offset and tilt relative to optical axis, undergoes multiple bounces before exiting. In this work, a multi-pass delay stage conceived for up to 100 reflections per mirror has been designed. Spherical mirrors with focal length f = 1 m, diameter d = 0.15 m and a 4.5x25 mm radial slit in one of the mirrors have been used. Optical coatings by Layertec GmbH provide high reflectivity (R > 99.9%) and nearly zero group delay dispersion (GDD) at the wavelengths λ = 780-820 nm. The slit width matches the beam diameter of the femtosecond laser exactly, in order to produce maximum optical path in the Herriott cell. The separation between two mirrors can be changed on the interval from L=f to L=2·f. In order to derive the general condition required to preserve the q parameter of the Gaussian beam, an arbitrary Herriott cell, an initial injected beam $\vec{r}_0$ and its transfer matrix M_T at a spherical mirror surface are considered:

$$\vec{r}_0 = \begin{pmatrix} r_0 \\ r_0' \end{pmatrix}, \quad M_T = \begin{bmatrix} 1 & 0 \\ -2/R & 1 \end{bmatrix}. \tag{1}$$

r_0 represents the initial beam displacement from the optical axis, r_0' is the initial entrance angle of the beam and R is the radius of curvature of the mirrors. After n bounces, the beam vector $\vec{r}_n$ becomes

$$\vec{r}_n = \begin{pmatrix} r_n \\ r_n' \end{pmatrix} = [M_1] \cdot [M_2] \cdots [M_n] \cdot \begin{pmatrix} r_0 \\ r_0' \end{pmatrix}. \tag{2}$$

Because of typically small entrance angles and very large radii of curvature of the mirrors, astigmatism resulting from the tilted beam can be neglected[7]. By using some basic techniques of matrix algebra, the transverse displacements x_n and y_n of the beam and the angular position θ of the spots around the ellipse formed after n successive bounces can be given:

$$x_n = A\sin(n\theta + \alpha), \quad y_n = B\sin(n\theta + \beta), \quad \cos\theta = 1 - \frac{L}{R}. \tag{3}$$

Thus, if A = B = R_H, a circle of radius R_H will be outlined by the bouncing beam. Parameters α and β can be then expressed:

Downloaded From: http://proceedings.spiedigitallibrary.org/ on 12/29/2015 Terms of Use: http://spiedigitallibrary.org/ss/TermsOfUse.aspx

$$\tan\alpha = \frac{\sqrt{\frac{4f}{L}-1}}{1+2f\frac{x_0'}{x_0}} \quad \text{and} \quad \beta = \alpha \pm \frac{\pi}{2}. \tag{4}$$

In order to preserve the q parameter of the Gaussian beam, for the specific case of $y_0' = 0$, following start conditions for the initial beam displacement and entrance angle can be given:

$$x_0 = R_H\sqrt{\frac{L}{4f}}, \quad x_0' = -\frac{R_H}{\sqrt{Lf}}. \tag{5}$$

In this specific case, in order to satisfy the periodic "re-entrance condition"[8] it has to be noted:

$$N\cdot\theta = 2\pi\cdot j, \quad L = 2f\left(1-\cos\frac{2\pi\cdot j}{N}\right). \tag{6}$$

N is the number of beam passes inside the Herriott cell, and *j* is an integer representing the circulation number of the spots around the circle. Using equations (3)-(6) precise calculations for the mirror separation length can be performed, according to required numbers of beam passes. Some examples of numerical beam tracing calculations are presented in Figure 2.

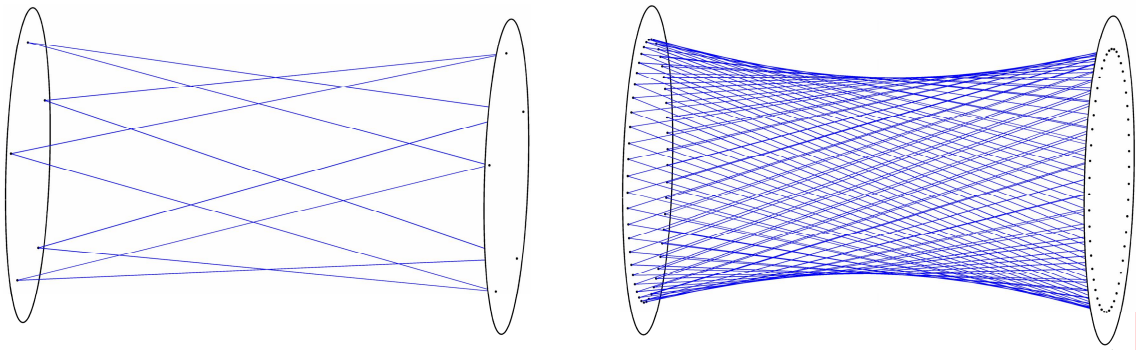

Figure 2. Beam tracing inside the Herriott cell for N=10, L=1382.0 mm (left), and N=100, L=1749.3 mm (right).

One of the dominating disadvantages of using a Herriott cell based delay stage with the femtosecond laser radiation consists in the periodic changing of the focus position inside the cell. When using large pulse energies, the mirror coatings can be damaged. The delay stage presented in this study has been tested at pulse energies up to E = 0.2 mJ and a pulse duration t_p = 80 fs. Therefore, in order to perform safe operations with the multi-pass delay stage, certain accuracy is required by choosing appropriate values of the pulse energy.

2.3 Femtosecond laser ablation shadowgraphy

A shadowgraph image (Figure 3, a) recorded with the CCD camera after a single pulse interaction with copper features an expanding hemispherical shock wave, a gas-like plume and material droplets. In addition to these characteristic phenomena, in the femtosecond laser ablation of copper and aluminium, a jet expanding vertically upward was observed in the later stages. Interference patterns resulting from the light scattering on the sample edges can be eliminated by dividing the initial intensity image (Figure 3, a) with the background intensity without the ablating irradiation (Figure 3,

Downloaded From: http://proceedings.spiedigitallibrary.org/ on 12/29/2015 Terms of Use: http://spiedigitallibrary.org/ss/TermsOfUse.aspx

b). The calculated spatial transmittance image (Figure 3, c) provides better contrast and reduction of artefacts. In the presented figures, the pump laser radiation enters the system from the top.

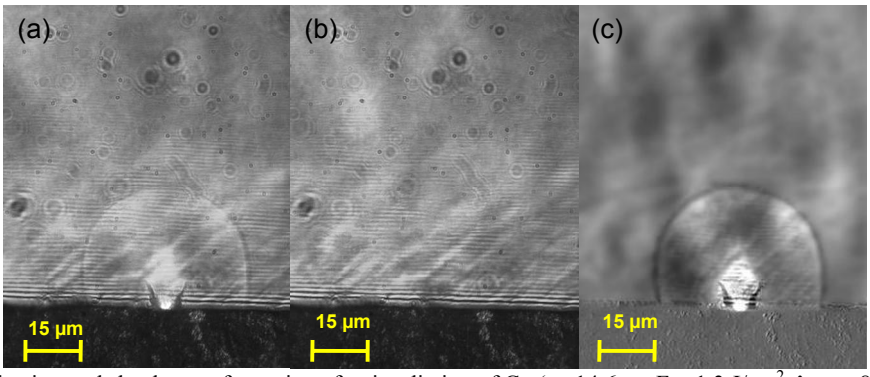

Figure 3. Melt ejection and shockwave formation after irradiation of Cu (τ =14.6 ns, F = 1.3 J/cm^2, λ_{pump}=820nm, t_p=80 fs): (a) shadowgraph image with pump irradiation, (b) background image without pump irradiation, (c) calculated spatial transmittance.

3. RESULTS AND DISCUSSION

3.1 Plasma and melt dynamics

In general, the interaction of high power pulsed laser radiation with solid materials involves complex phenomena, e.g. of optical, thermal, mechanical or hydrodynamic nature. During the first instants of the interaction the incident energy is distributed among these phenomena. For this study, using ultrafast laser radiation in the near-infrared wavelength range, linear and two-photon absorption are assumed to be dominant absorption mechanisms[9]. A part of the initial energy is absorbed leading to the heating of the bulk. Then, the melting and the vaporization of the irradiated sample can be observed.

The time-resolved images (Figure 4) indicate evolution of the ablation dynamics in aluminium starting at around 3.0 ns after the irradiation of the sample. The measurements were performed with white light continuum as the probe laser radiation. Energetic electrons overcoming the work function of the metal can escape from the target. Consequently, the electric field created by the charge separation between the escaping electrons and parent ions effectively could pull ions out of target. Thus, the energetic fast ions[10] are likely emitted via a non-thermal process during the early stage of ablation in the time range up to some nanoseconds. It should be noted, however, that the net surface charge density due to non-thermal process was reported to be two orders of magnitude lower than in dielectric materials[11]. Gradual darkening of the central portion of the irradiated area was observed at small elapsed times τ < 3.0 ns due to the emergence of a thin plasma layer in the proximity of the sample surface that attenuates the probe laser beam.

Qualitatively, the plasma and melt dynamics presented in Figure 4 complies with some well-known theoretical issues[12] based on the molecular dynamics assumptions. In this experiment, however, to be contrary to the performed calculations, significant differences in the time scales of dynamic processes can be observed due to unlike focusing conditions and different applied pulse energy. According to the theoretical and experimental data on ablation dynamics of solids by K. Sokolowski-Tinten[13,14] et al., the expansion starts with a rarefaction wave that proceeds from the surface into the material. After reflection at the unperturbed substrate the rarefaction wave travels towards the surrounding atmosphere. This results in a thin layer of high density, which is moving away from the target in front of a low density region. The low density region is assumed to be a liquid-gas mixture caused by homogenous nucleation within a few tens of picoseconds.

Few groups[15,16] reported theoretical and experimental works on ablation mechanisms of metals and semiconductors on nanosecond timescales and longer by evaporation and “normal boiling” effects after heterogeneous nucleation. Calculations[17] performed for metals above the boiling temperature, however, result in a removal of only several atom layers in 100 ns. Therefore, this process seems to be negligible for short timescales. Concerning boiling effects, heterogeneous nucleation in the liquid is involved. Calculations for metals at twice the melting temperature result in

Downloaded From: http://proceedings.spiedigitallibrary.org/ on 12/29/2015 Terms of Use: http://spiedigitallibrary.org/ss/TermsOfUse.aspx

diffusion distances <1 nm in 100 ns. Therefore, normal boiling is also not expected to have significant contribution to the ablation for the time scale <1 μs. Experiments on GaAs below the plasma formation threshold[14], however, show bubble-like structures in the liquid. These bubbles appear about 20 ns after the ablation pulse and grow linear in time.

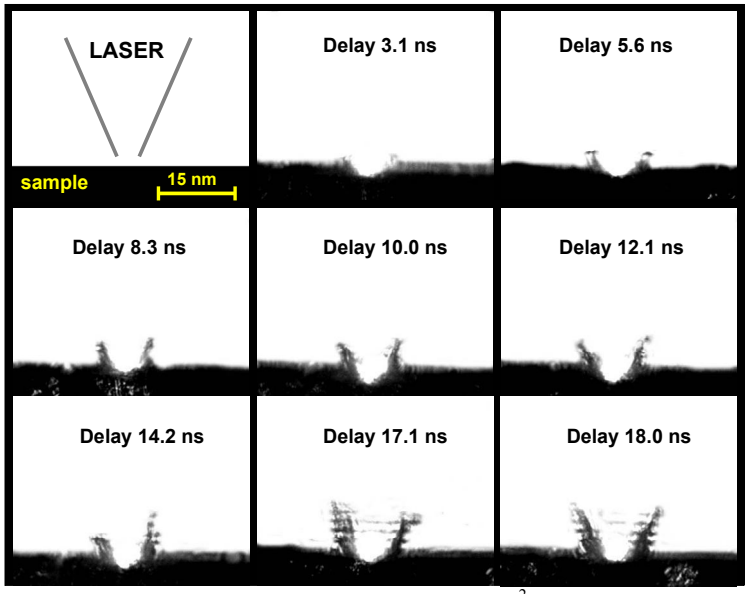

Figure 4. Plasma and melt dynamics on Al target (F = 1.4 J/cm^2, λ_{pump}=820nm, t_p=80 fs, WLC).

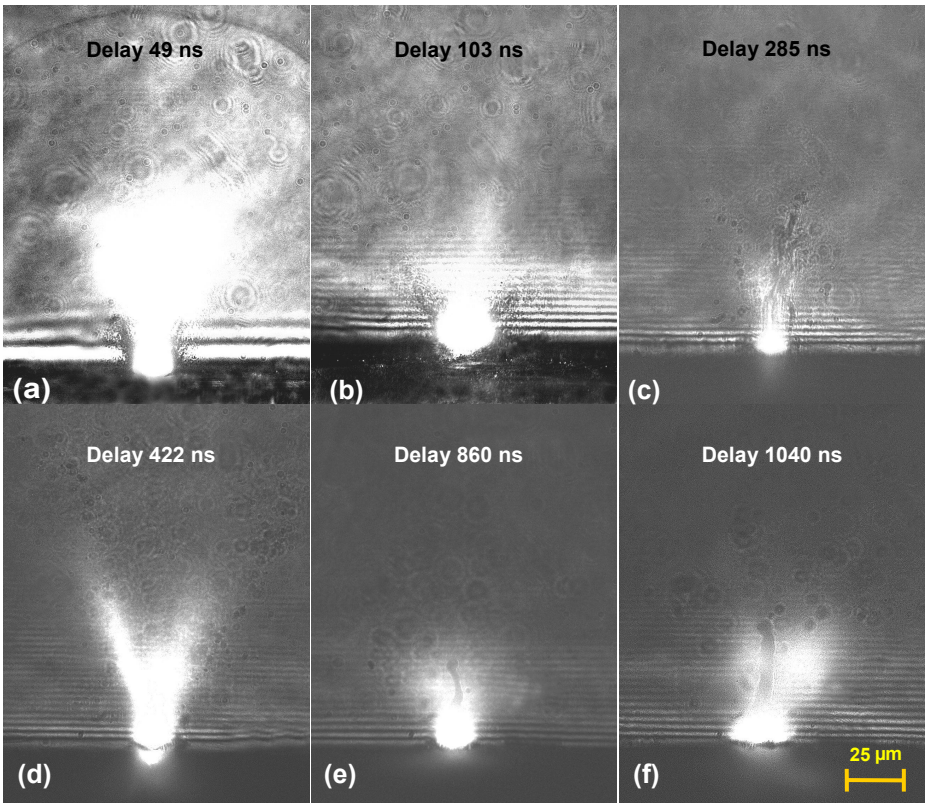

Figure 5. Ejection of plasma and melt from Al target (F = 1.8 J/cm^2, λ_{pump}=820nm, t_p=80 fs, WLC).

Downloaded From: http://proceedings.spiedigitallibrary.org/ on 12/29/2015 Terms of Use: http://spiedigitallibrary.org/ss/TermsOfUse.aspx

The dynamics of the melt formation and material ablation for single pulse irradiation at longer pump-to-probe elapsed times up to τ = 1.04 µs (Figure 5) reveals a variety of phenomena, like plasma formation, ejection of material droplets and liquid jets. At the delay τ = 49 ns (Figure 5, a) an expanding shockwave can be clearly observed.

The experimental data shows that the phenomenological development of the ablation dynamics on the time delay range between τ = 3.0 ns and τ = 1.04 µs can be conditionally categorized into three characteristic time regions. The first one features photo-induced emission, formation and expansion of highly pressurized, heated material, combined with the beginning formation of shockwaves (Figure 4 and Figure 5 a-b). This expansion of shockwaves and vapor plume in gas can be described by a combined model developed for nanosecond ablation[15,16].

Starting at approximately τ = 200 ns (Figure 5, c-d), the ablated material is ejected explosively. Observation of similar dimensions (approx. 1 – 3 µm) of ejected droplets and material particles can be measured for metals Cu and Fe. This behavior has to be related to the aforementioned nucleation effects[17].

During the third characteristic time region at time delays τ > 700 ns (Figure 5, e-f), a jet of molten material expanding vertically upward was observed on aluminium targets. The estimated height of the ejected structures averages about 50 µm at the delay τ = 1.04 µs. Because of the relative small electron-phonon coupling constant of aluminium $\mu = 4.1 \cdot 10^{16}$ W m^{-3} K^{-1}, these results can be compared to the works on nanojets and microbumps formation on gold films by Corte et al[18].

3.2 Structural analysis of ablated material

Depending on the fluence of the laser radiation, qualitative differences of the performed surface modifications in copper and aluminium (Fig. 6 a and b) occurred. The surface morphology of copper (a) reveals rosette-like modifications. Solidified melt droplets and material jets on sub-micrometer size scale can be seen in the distance of some 5-10 µm from the center of the ablated region. Slightly elliptical contours of the produced craters correspond to the beam profile of the used laser radiation. In contrast to that, the crater contours on aluminium targets retain sharp edges.

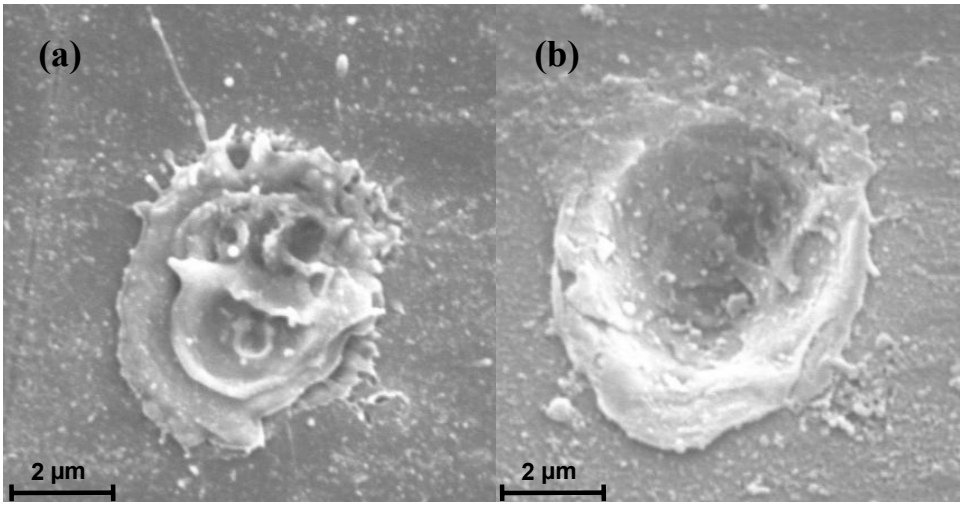

Figure 6. Results of the surface structuring by single pulse laser interaction with metals, at t_p=80 fs, λ=820 nm .
(a) Cu, F = 0.4 J/cm^2, (b) Al, F = 0.3 J/cm^2.

4. CONCLUSIONS

A novel pump-probe setup designed in this work and deploying a low-loss multi-pass delay stage, enables time-resolved observation of ablation phenomena up τ = 1.2 µs after the irradiation of the sample with high temporal and spatial resolution.

Downloaded From: http://proceedings.spiedigitallibrary.org/ on 12/29/2015 Terms of Use: http://spiedigitallibrary.org/ss/TermsOfUse.aspx

Presented shadowgraphs provide direct visualization of plasma and melt development on the time scale up to 1.04 μs after the initial laser-material interaction. Being in accordance with some theoretical issues on ablation by ultrashort laser radiation, observed ablation dynamics implies processes with emission of particles, vapour and melt up to several hundred nanoseconds after the laser pulse in at least three characteristic time regions. The phenomenology during the first ablation stage includes expansion of highly pressurized, heated material and up to 200 ns after the material irradiation. An explosion-like emission of melt droplets with diameter smaller than 3 μm can be observed at delays up to 700 ns, which has been also reported by some groups. Finally, a massive melt ejection at time delays larger than approximately 700 ns occurs.

5. ACKNOWLEDGEMENTS

We acknowledge financial support for the research by the German Research Society (DFG) within the priority program SPP 1139.

REFERENCES

1. N.N. Nedialkov, S.E. Imamova, P.A. Atanosov, Ablation of metals by ultrashort laser pulses, J. Phys. D: Appl. Phys. 37, 638 (2004)
2. P. Mannion, J. Magee, E. Coyne, G.M. O'connor, Ablation thresholds in ultrafast laser micro-machinihg of common metals in air, Proceedings SPIE. 4876, 470 (2003)
3. J.Krüger und W.Kautek, Femtosecond-pulse laser processing of metallic and semiconducting thin films, Proceeding SPIE 2403, 436 (1995)
4. J. Ihlemann, A. Scholl, H. Schmidt, B. Wolff-Rottke, Nanosecond and femtosecond excimer laser ablation of oxide ceramics, Appl. Phys. A 60, 411 (1995)
5. S. Campbell, F.C. Dear, D.P. Hand, D.T. Reid, Single-pulse femtosecond laser machining of glass, J. Opt. A 7, 162 (2005)
6. J. Krüger, W. Kautek, Femtosecond pulses visible laser processing of fibre composite materials, Appl. Surf. Sci. 106, 383 (1996)
7. A. E. Siegman, An Introduction to Lasers and Masers, McGraw-Hill (1970)
8. D. Herriott, H. Kogelnik, and R. Kompfner. Off-Axis Paths in Spherical Mirror Interferometers. Appl. Opt., 3 , 523 (1964)
9. R. Hermann, J. Gerlach, and E. Campbell, Ultrashort pulse laser ablation of silicon: an MD simulation study, Appl. Phys. A 66, 35 (1998)
10. F. Dausinger, F. Lichter and H. Lubatschowski, Femtosecond Technology for Technical and Medical Applications, Springer, Heidelberg (2004)
11. R. Stoian, A. Rosenfeld, D. Ashkenasi, I. V. Hertel, N. M. Bulgakova and E. E. B. Campbell, Surface Charging and Impulsive Ion Ejection during Ultrashort Pulsed Laser Ablation, Phys. Rev. Lett. 88, 097603 (2002)
12. Danny Perez and Laurent J. Lewis, Ablation of Solids under Femtosecond Laser Pulses, Phys. Rev. Lett. 89, 255504 (2002)
13. K. Sokolowski-Tinten, J. Bialkowski, A. Cavalleri, M. Boing, H. Schüler and D. von der Linde, Dynamics of femtosecond laser induced abaltion from solid surfaces, Proc. SPIE 3343, 46 (1998)
14. K. Sokolowski-Tinten, J. Bialkowski, M. Boing, A. Cavalleri and D. von der Linde, Bulk phase explosion and surface boiling during short pulse laser ablation of semiconductors, OSA Technical Digest, 231 (1999)
15. J. König, S. Nolte and A. Tünnermann, Plasma evolution during metal ablation with ultrashort laser pulses, Optics Express, 13, No. 26, 10597 (2005)
16. D. Bäuerle, Laser Processing and Chemistry, 3rd ed., (2000)
17. R. Kelly and A. Miotello, Contribution of vaporization and boiling to thermal-spike sputtering by ions or laser pulses, Phys. Rev. E 60, 2616 (1999)
18. F. Korte, J. Koch, B.N. Chichkov, Formation of microbumps and nanojets on gold targets by femtosecond laser pulses, Appl. Phys. A 79, 879 (2004)

Downloaded From: http://proceedings.spiedigitallibrary.org/ on 12/29/2015 Terms of Use: http://spiedigitallibrary.org/ss/TermsOfUse.aspx